# High-precision first-order reversal curve (FORC) functions for single-domain ferromagnets with uniaxial anisotropy

Andrew J. Newell
*Center for Research in Scientific Computation, Department of Marine, Earth and Atmospheric Sciences, P.O. Box 8208, North Carolina State University, Raleigh, NC 27695-8208**

Plots of the first-order reversal curve (FORC) function are used to characterize ferromagnetic particles in rocks. The function is based on classical Preisach theory, which represents magnetic hysteresis by elementary loops with displacement $H_u$ and half width $H_c$. In this article it is shown that in general there are two FORC functions that are related by reflection across the $H_c$ axis. The choice of FORC function depends on the sequence of magnetic measurements. Using analytical and numerical integration of single-particle magnetization curves, a high-precision FORC function is calculated for a sample with randomly oriented, noninteracting, elongated single-domain particles. Their orientations are taken from a bimodal (Dimroth-Watson) distribution and their aspect ratios from a lognormal distribution. The function has a positive peak on the $H_c$ axis and a negative peak on the $H_u$ axis. The peaks are at equal distances from the origin, but the positive peak is larger. The relative size of the peaks is determined mainly by the easy axis anisotropy while their shapes are determined by the aspect ratio distribution. If the latter distribution is narrow there is a ridge slanting between the peaks. If it is broad there a broad hump roughly centered around each peak. The model results are compared with a FORC function for a magnetic tape. Most of the main features are reproduced. The most notable exception is a spreading of the positive peak to $H_u > 0$ in the function for the magnetic tape. This is probably due to nonuniform magnetization. A particle can have nonuniform magnetization in a remanent state even though it is considered single-domain because of its saturation remanent state.

## I. INTRODUCTION

Rock magnetists and environmental magnetists use magnetic hysteresis measurements to characterize ferromagnetic minerals in rocks and sediments. Many labs represent the hysteresis by a few well-known parameters: the saturation magnetization $M_s$, the saturation remanence $M_{rs}$, the coercivity $H_c$, and the coercivity of remanence $H_{rc}$[5]. These parameters can be summarized in a plot of $M_{rs}/M_s$ against $H_{rc}/H_c$[3]. This "Day" plot is a standard tool for estimating mineral size, but its interpretation is highly ambiguous. One reason for ambiguity is that samples are often mixtures of simpler components. Suites of samples with varying ratios of components often follow trends on the Day plot[11,23,35]. However, each sample is represented by only one data point. This provides little information on the components, which are themselves collections of particles with distributions of physical properties. More detailed information on each sample can be obtained using isothermal remanence curves, which can be considered one-dimensional profiles through the hysteresis[6,30]. Now plots of the FORC function provide two-dimensional profiles[26].

The FORC function is a measure of the rate of irreversible change in magnetization. It is determined by a set of magnetization curves called first-order reversal curves (FORCs), as in Fig. 1. Where there is no hysteresis it is zero. The relationship between to FORCs and FORC functions is derived in classical Preisach theory[13], where the latter is called the Preisach function or distribution. The same relationship can still be used to determine the FORC function even where the theory does not apply (but see Section II A). In plots of the FORC function one can identify multiple components in a sample[29] and compare the components with FORC plots for relatively well-characterized samples[18,26].

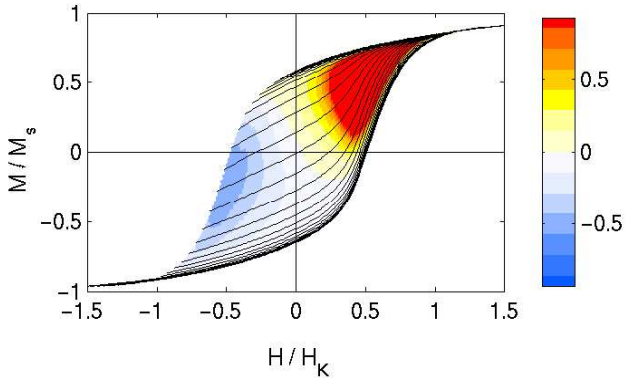


FIG. 1: Black lines: first-order reversal curves (FORCs) for a high-density magnetic tape (courtesy of Chris Pike). Magnetic fields are normalized by $H_K$, the field at which the loop closes. The magnetic moment is normalized by the saturation magnetization $M_s$. For clarity, only a subset of the 140 curves are shown. Color image: the normalized FORC function (derived using a method similar to that described in[26]). The top of the color scale is truncated to make the negative region visible (see also Fig. 3).

The FORC function has mainly been used to obtain qualitative information on the components. Although there has been some theoretical modeling of FORC

functions[26,27,33], quantitative predictions have not been compared with experiment. Most FORC plots do not even have scale bars on them. The magnitude of the FORC function is not very meaningful unless the volume of the magnetic component is known. However, if there is only one component the magnetization and field can be normalized as in Fig. 1 to get a normalized FORC function.

The magnetic tape in Fig. 1 is probably composed of elongated particles of maghemite or cobalt-doped maghemite[15]. (Unfortunately, the details are proprietary.) The ratio of saturation remanence to saturation magnetization is $M_{rs}/M_s = 0.62$, indicating that the particles are single-domain (SD) with some anisotropy to their orientations (Section III C). SD particles play a central role in rock magnetism[5] and there are many important examples of rocks with elongated SD particles. These include magnetite inclusions in pyroxenes[7], plagioclase[31] and ash flow tuffs[29]. Such particles tend to carry a particularly stable natural remanent magnetization (NRM). As described in Section II A, the FORC function for SD particles has several distinct features, none of which have been fully explained.

In this article I calculate FORC functions for systems of single-domain particles with uniaxial anisotropy. The calculations include the effects of random distributions of particle orientations (isotropic or anisotropic) and distributions of particle shapes. A lot of the work is carried out analytically, allowing high-accuracy calculations. I will also use the analytical expressions to explain the main features of the FORC function in terms of the component particles. And I will compare the theory to the FORC function for the magnetic tape.

## II. BACKGROUND

In this section I describe some of the theory behind the FORC function and some previous work on FORC functions in single-domain systems. Then I describe the classic model for single-domain particles, the Stoner-Wohlfarth model. This model will be the starting point for the calculations in the Section III.

### A. The FORC function

First-order reversal curves (FORCs) can be measured in one of two ways (Fig. 2). The FORCs in Fig. 1 were obtained by decreasing the field from a large positive field to a minimum field $H'_a$, and then measuring the magnetization at an increasing series of fields $H'_b$. A set of measurements $M(H'_a, H'_b)$, with fixed $H'_a$ and $H'_a \leq H'_b$, is called an increasing FORC[14]. Decreasing FORCs ($M(H''_a, H''_b)$ in Fig. 2) start at negative saturation and are used in most applications of Preisach theory.

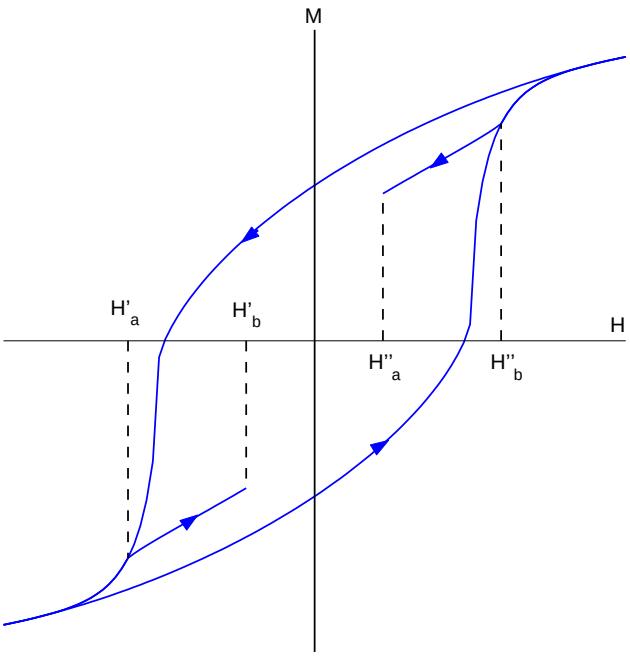


FIG. 2: Two types of first-order reversal curves. An increasing FORC is the curve $M(H'_a, H'_b)$, with $H'_a$ fixed and $H'_b > H'_a$. A decreasing FORC is $M(H''_a, H''_b)$ with $H''_b$ fixed and $H''_a < H''_b$.

[14] showed that the FORC function can be derived from the FORCs using either

$$\mu(H_a, H_b) = -\frac{1}{2}\frac{\partial^2 M(H_a, H_b)}{\partial H_a \partial H_b} \tag{1}$$

for increasing FORCs, or

$$\mu(H_a, H_b) = \frac{1}{2}\frac{\partial^2 M(H_a, H_b)}{\partial H_a \partial H_b} \tag{2}$$

for decreasing FORCs. I show in Section IV A that the two functions are equal if and only if classical Preisach theory correctly predicts the hysteresis. Otherwise, one should distinguish between increasing and decreasing FORC functions. Unless I state otherwise, I use "FORC function" to refer to the increasing FORC function.

The FORC function is often converted to $(H_c, H_u)$ coordinates, where $H_u = (H_b + H_a)/2$ and $H_c = (H_b - H_a)/2$. In some publications $\mu$ is multiplied by a factor of two, but I will use the same $\mu$ for both sets of coordinates. Since it is simpler to derive expressions for $\mu(H_a, H_b)$ and trivial to convert to $\mu(H_c, H_u)$, I mostly give explicit expressions in terms of $H_a$ and $H_b$.

Preisach modelers generally make *a priori* assumptions about the form of the FORC function. A common one is that $\mu(H_c, H_u) = P(H_c)Q(H_u)$ where $P$ and $Q$ are proportional to normal probability density functions[4,32,36]. Until recently it was hard to judge such assumptions because the only plots of the FORC function were plots of the *a priori* function with parameters fitted to the data.

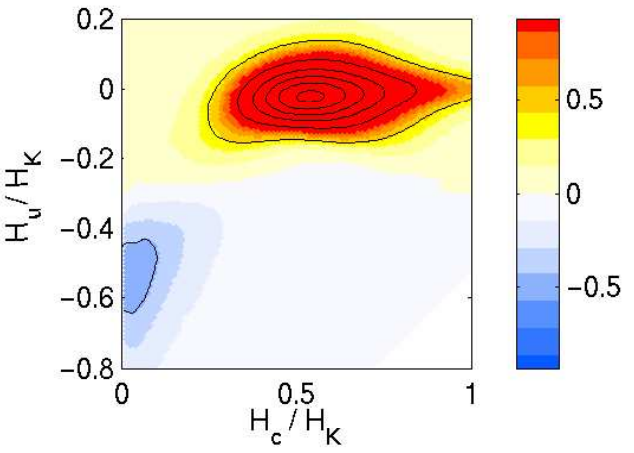


FIG. 3: The FORC function from Fig. 1, redrawn in normalized $(H_c, H_u)$ coordinates. The color scale is restricted to $[-1, 1]$ to emphasize the negative region. The black contours are six times farther apart than the color contours and cover the entire range of $\mu$. No data were collected in the white region.

[26] showed how to use polynomial fits to get unconstrained estimates of the FORC function. This allows direct comparisons between the function and the assumptions of Preisach modelers. For example, the FORC function in Fig. 1 cannot be a probability distribution because it is negative over much of the left half of the hysteresis loop. Similar negative regions are seen in other single-domain samples[1,25,26].

If the FORC function is plotted in $(H_c, H_u)$ coordinates (Fig. 3), the negative region rises to a ridge along the negative $H_u$ axis and the positive region peaks near the positive $H_c$ axis. The negative and positive regions are at the same distance from the origin, but the positive peak is higher.

Negative regions have been attributed to particle interactions[26,33]. However,[17] also see them in numerical models of noninteracting single-domain particles, so particle interactions can not be the sole reason for the negative regions.[17] attribute the negative region to a systematic decrease, for a given $H_b < 0$, in the slopes of the FORCs as $H_a$ decreases. However, it is not clear why this decrease occurs or why similar negative regions are not seen in non-SD samples.

The FORC function has other features that have not been adequately explained. Why are the positive and negative regions roughly symmetric about the $H_u = -H_c$ axis but so different in magnitude? Also, the positive region in[17] (their Fig. 2) has a boomerang shape. (The negative region probably has a boomerang shape as well, but the axes do not extend far enough.) Why does the boomerang have a 135° internal angle? And why is this shape not seen in the experimental FORC diagram (Fig. 3)? In this article I answer these questions by relating the FORC function for a large number of particles to the magnetic hysteresis of the component particles.

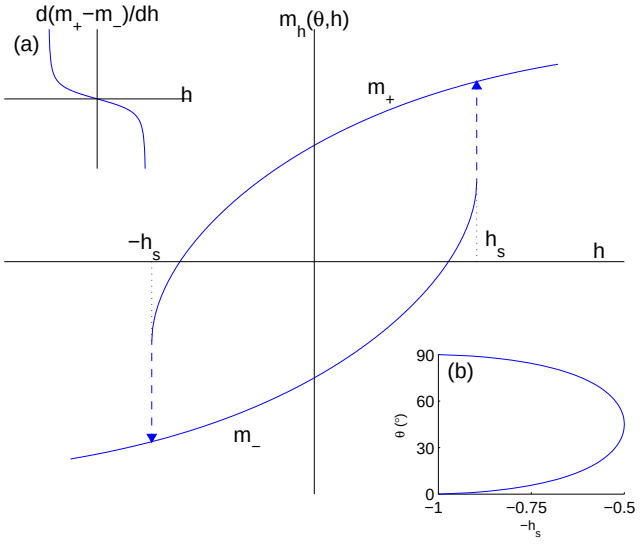


FIG. 4: Main plot: The solid curves are the stable solutions $m_\pm$ of the Stoner-Wohlfarth model for an angle $\theta = 60°$. The jumps at the switching fields $\pm h_s$ are shown as dashed lines with arrows indicating the directions of the jumps. Inset (a): Difference between the derivatives of the solution curves $(f_h = d/dh(m_+ - m_-))$ . Inset (b): The relationship between switching field and the angle $\theta$ between field and easy axis.

### B. The Stoner-Wohlfarth Model

The model of[34] predicts the magnetic hysteresis for single-domain particles with a uniaxial anisotropy (having a single preferred axis for magnetization in zero field).

Let $\theta$ be the acute angle between the field and the easy axis. Let $\phi$ be the angle between the positive field direction and the magnetization. The energy for a given pair of angles $\theta$ and $\phi$ is (in SI units)

$$E = K_u V \sin^2(\phi - \theta) - \mu_0 M_s H V \cos\phi, \qquad (3)$$

where $K_u$ is a parameter representing the magnitude of the anisotropy. This can have more than one physical origin. If the anisotropy is a magnetostatic anisotropy due to particle elongation then $K_u = (1/2)\mu_0 N M_s^2$, where $N$ is the shape-dependent demagnetizing factor (see Appendix A) and $M_s$ the saturation magnetization.

Define an anisotropy field $H_K = 2K_u/\mu_0 M_s$, a reduced field $h = H/H_K$, and a reduced energy

$$\eta = \frac{1}{2}\sin^2(\phi - \theta) - h\cos\phi. \qquad (4)$$

An equilibrium solution for $\phi$ satisfies $d\eta/d\phi = 0$ and it is stable if $d^2\eta/d\phi^2 > 0$. For a given field angle $\theta$ there are two stable solutions $m_h = \cos\phi = m_\pm(\theta, h)$ for the component of magnetization in the direction of the field (e.g., Fig. 4).

When the magnetization reaches the end of the upper curve it becomes unstable and jumps to the lower

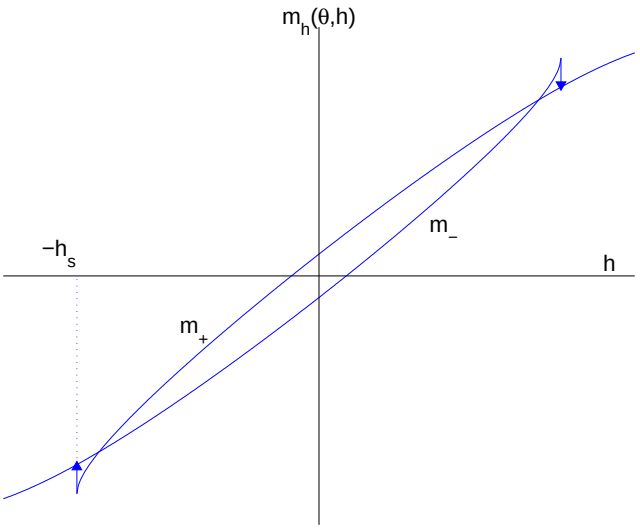


FIG. 5: Hysteresis of a Stoner-Wohlfarth particle with $\theta = 85°$. The solution curves cross each other and the jump at $h = -h_s$ is upward.

curve. The magnitude of the field at which this occurs, the switching field, is[34]

$$h_s = \frac{\sqrt{1 - t^2 + t^4}}{1 + t^2}, \tag{5}$$

where $t = \tan^{1/3}\theta$. The dependence of $h_s$ on $\theta$ is shown in Fig. 4b.

For each field $h \in [-1, -0.5]$ there are two angles $\theta \in [0, \pi/2]$ such that $h$ is a switching field. These are $\theta_s$ and $\pi/2 - \theta_s$, where[34]

$$\theta_s(h) = h_s^{-1}(h) = -\arctan\left[\frac{\sqrt{3} - \sqrt{4h^2 - 1}}{2\sqrt{1 - h^2}}\right]^3. \tag{6}$$

Aside from the special cases $\theta = 0$ and $\theta = \pi/2$, the slope $dm_+/dh$ approaches infinity as the field approaches the jump. The slope can be obtained most easily by solving $d\eta/d\phi = 0$ for $h$ and taking the derivative of $h$ with respect to $\phi$:

$$\frac{dm_+}{dh} = -\frac{dm_h/d\phi}{dh/d\phi} = \frac{\sin 3\phi - 3\sin\phi}{\sin(2\theta - 3\phi) - 3\sin(2\theta - \phi)}. \tag{7}$$

The difference between the slopes of the upper and lower curves is plotted in Fig. 4a. The difference is zero for $|h| > h_s$, while for $-h_s < h < h_s$ it goes from $+\infty$ to $-\infty$ as $h$ increases.

The jump in magnetization at the switching field is generally downward, but for $\theta > 76.7°$ it is upward. An example of an upward jump is shown in Fig. 5. Before the jump the curves $m_+$ and $m_-$ cross each other, so "upper" and "lower" trade places. This prediction of Stoner-Wohlfarth theory is not well known. In Fig. 6 of[34] a positive jump occurs for the $\theta = 80°$ solution, but it is very small and obscured by other lines.

In real units, the switching fields range from $0.5H_K$ to $H_K$. Thus, in a set of randomly oriented Stoner-Wohlfarth particles, the collective hysteresis loop closes at $H = H_K$ (compare Fig. 1). If all easy axis directions are equally likely the saturation remanence is $0.5M_s$ and the coercivity is $0.479H_K$[34].

## III. RESULTS

In this section I derive the (increasing) FORC function for increasingly complex systems of Stoner-Wohlfarth particles. These are a single oriented particle (Section III A), randomly oriented identical particles (isotropic in Section III B and anisotropic in Section III C), and randomly oriented particles with a distribution of shapes (Section III D). Then, in Section III E I compare the predictions with the FORC function for the magnetic tape.

### A. Single Particle

For a single particle or a set of identical particles one can normalize the fields as in Section II B and define a normalized FORC function

$$\tilde{\mu}(\theta, h_a, h_b) = \frac{H_K^2}{M_s}\mu(\theta, H_a, H_b), \tag{8}$$

where $h_a = H_a/H_K$ and $h_b = H_b/H_K$. Then

$$\tilde{\mu}(\theta, h_a, h_b) = -\frac{1}{2}\frac{\partial^2 m_h}{\partial h_a \partial h_b}. \tag{9}$$

Consider a Stoner-Wohlfarth particle with angle $\theta$ between field and easy axis (Fig. 4). If the field starts at a large positive value, decreases to $h_a$, and then increases to $h_b$, the magnetization is given by

$$m_h(\theta, h_a, h_b) = \begin{cases} m_+(\theta, h_b) & \text{if } h_a > -h_s(\theta) \text{ or } h_b > h_s(\theta), \\ m_-(\theta, h_b) & \text{if } h_a < -h_s(\theta) \text{ and } h_b < h_s(\theta). \end{cases} \tag{10}$$

Note that $m_h$ is not defined at the discontinuities ($h_a = -h_s$ and $h_b = h_s$).

This can be expressed in terms of the Heaviside function $\Theta(x)$, which is defined as $\Theta(x) = 0$ for $x < 0$ and $\Theta(x) = 1$ for $x > 0$ and is undefined for $x = 0$:

$$\begin{aligned} m_h(\theta, h_a, h_b) = {} & m_+(\theta, h_b)\left[1 - \Theta(-h_a - h_s)\Theta(-h_b + h_s)\right] \\ & + m_-(\theta, h_b)\Theta(-h_a - h_s)\Theta(-h_b + h_s). \end{aligned} \tag{11}$$

Then

$$\frac{\partial m_h}{\partial h_a}(\theta, h_a, h_b) = \delta(h_a + h_s)\Theta(-h_a - h_b)f(\theta, h_b), \tag{12}$$

where $\delta(x)$ is the Dirac delta function and $f(\theta, h) \equiv m_+(\theta, h) - m_-(\theta, h)$ is the difference between the upper and lower curves.

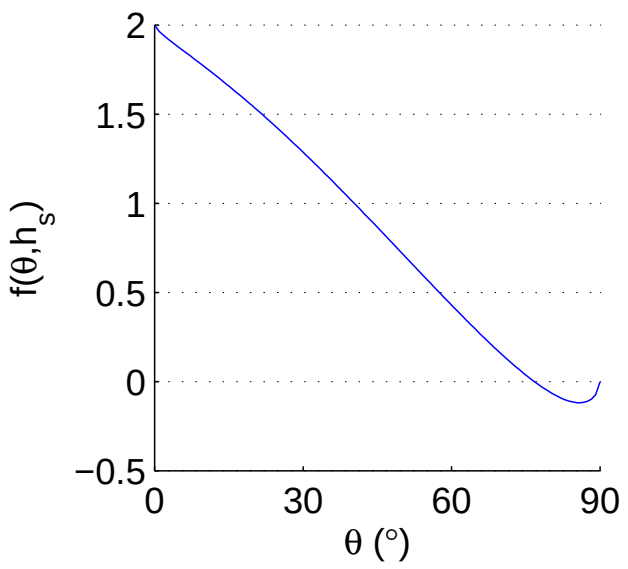


FIG. 6: The normalized jump in magnetization at the switching field as a function of easy axis direction.

The value of $f(\theta, h)$ at $h = h_s$ is the size of the jump from the lower curve to the upper curve. At $\theta = 0$ this is equal to 2, the difference between positive and negative saturation in normalized coordinates. As $\theta$ increases the magnitude of the jump decreases (Fig 6). At angles of $\theta$ near $\pi/2$ it is negative, as in Fig. 5.

Taking the derivative of (12) with respect to $h_b$ and using (1), we get

$$\tilde{\mu}(\theta, h_a, h_b) = \frac{1}{2}\delta(h_a + h_s)\delta(h_a + h_b)f(\theta, h_b) - \frac{1}{2}\delta(h_a + h_s)\Theta(-h_a - h_b)f_h(\theta, h_b). \tag{13}$$

The first term represents the jump at $h_b = -h_a = h_s$, so $f(\theta, h_b)$ can be replaced by $f(\theta, h_s)$. In the other term $f_h(\theta, h_b)$ is the difference between the slopes of the curves (e.g., Fig. 4a). Each slope is a measure of reversible change, but the difference is the result of a jump from one curve to the other. Information on the slope of either curve by itself is lost.

### B. Average over random orientations (isotropic)

Consider a collection of randomly oriented, identical Stoner-Wohlfarth particles. Assume that all easy axis orientations are equally likely. If $\tilde{\mu}(\theta, h_a, h_b)$ is the normalized FORC function for a given angle $\theta$ (equation 13), the average $\tilde{\mu}$ is given by the integral over a half sphere:

$$\tilde{\mu}(h_a, h_b) = \int_0^{\pi/2} \tilde{\mu}(\theta, h_a, h_b) \sin\theta d\theta. \tag{14}$$

To calculate this integral one must express the delta function $\delta(h_a + h_s)$ in (13) as a function of $\theta$. This can be done using the identity[16] (p. 469)

$$\delta(p(x)) = \sum_n \frac{1}{|p'(x_n)|}\delta(x - x_n), \tag{15}$$

for a function $p(x)$ with zeros $x_n$. The prime denotes a derivative. The condition $p'(x_n) \neq 0$ must be satisfied or the delta function is meaningless.

Let $p(\theta) = h_a + h_s(\theta) = h_a + \theta_s^{-1}(\theta)$. For $-1 < h_a < -1/2$ the roots of $p$ are $\theta_a \equiv \theta_s(h_a)$ and $\pi/2 - \theta_a$, where $\theta_s$ is given by (6). Using the inverse function theorem,

$$\frac{1}{p'(\theta_a)} = \frac{1}{(\theta_s^{-1})'(\theta_a)} = \theta_s'(\theta_s^{-1}(\theta_a)) = \theta_s'(h_a). \tag{16}$$

Combining (15) and (16) we get the required transformation

$$\delta(h_a + h_s) = |\theta_s'(h_a)| \left(\delta(\theta - \theta_a) + \delta(\theta - \pi/2 + \theta_a)\right). \tag{17}$$

With this substitution, the result of the integration is

$$\tilde{\mu}(h_a, h_b) = \alpha(h_a)\delta(h_a + h_b) + \beta(h_a, h_b)\Theta(-h_a - h_b), \tag{18}$$

where

$$\alpha(h_a) = \frac{|\theta_s'(h_a)|}{2}\left[g(\theta_a, h_a) + g(\frac{\pi}{2} - \theta_a, h_a)\right] \tag{19a}$$

$$\beta(h_a, h_b) = -\frac{|\theta_s'(h_a)|}{2}\left[g_h(\theta_a, h_b) + g_h(\frac{\pi}{2} - \theta_a, h_b)\right] \tag{19b}$$

$$g(\theta, h) = f(\theta, h)\sin\theta. \tag{19c}$$

These equations only apply in the trapezoidal region $-1 \leq h_a \leq -1/2$ and $h_a \leq h_b \leq -h_a$, outside of which the function is zero.

The original function $\mu$ can be recovered from $\tilde{\mu}$ using (8):

$$M_s\mu(H_a, H_b) = A(H_a)\delta\left(\frac{H_a + H_b}{H_K}\right) + B(H_a, H_b)\Theta(-H_a - H_b), \tag{20}$$

where $A(H_a) = r^2\alpha(h_a)$, $B(H_a, H_b) = r^2\beta(h_a, h_b)$, and $r = M_s/H_K$. Multiplying $\mu$ by $M_s$ makes it dimensionless.

The coefficients $A$ and $B$ are plotted in Fig. 7a. $A$ has an asymptote at $H_c = 0.5H_K$. This occurs because the switching fields are concentrated near $h_a = -1/2$, and the derivative $\theta_s'(h)$ approaches infinity at $h = -1/2$ (Fig. 4b). $A$ also has a negative region between $0.806H_K$ and $H_K$. This field range corresponds to angles between 86.5° and 90°. This is only part of the range of angles (76.7° to 90°) for which the jump at $h_s$ is negative. The narrowing of the range occurs because the same switching fields are possessed by particles in a complementary range of small angles [0°, 22.3°]. In these particles the jumps are downward and larger in magnitude than the upward

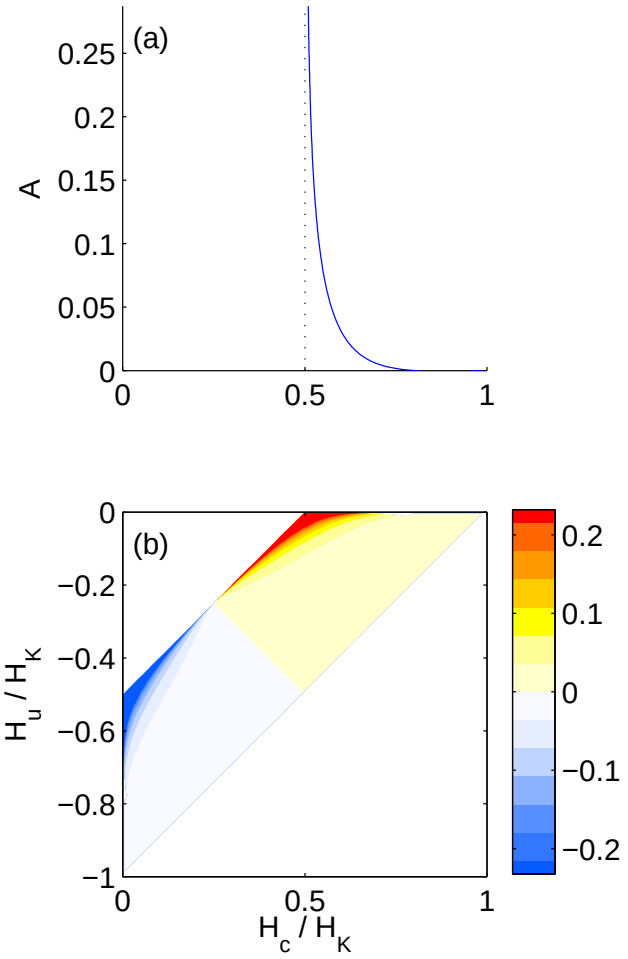


FIG. 7: The components of the FORC function for an isotropic sample of identical particles with aspect ratio $q = 2$. (a) $A$, representing jumps in magnetization. (b) $B$, representing changes in the slope of the magnetization curve. $B$ is zero outside of the colored region. A narrower color scale is used than in Fig. 3.

jumps. However, on a sphere small angles of $\theta$ occupy less solid angle. Thus, downward jumps dominate until the ratio between solid angles offsets the ratio of jump sizes. The negative swing in $A$ is too small to see in Fig. 7a.

The component $B$ contains the derivative $f_h$ and therefore represents differences between slopes of the upper and lower curves of each particle. Since the functions $\sin\theta_a$, $\cos\theta_a$ and $|\theta'_a|$ are always positive, $B$ and $f_h$ have opposite signs. Near the $H_u$ axis, as $H_b$ approaches $H_a$ the slope of the upper curve approaches infinity while the slope of the lower curve stays finite. Thus, $B$ approaches negative infinity. Near the $H_c$ axis the roles are reversed and $B$ approaches positive infinity. This asymptote is at $H_b = -H_a$ because the jumps in Stoner-Wohlfarth particles are symmetrically placed about $H = 0$. Other kinds of ferromagnets do not have this symmetry.

$B$ has an asymptote at $H_a = -H_K/2$ for the same reason that $A$ does. This is a line at a 45° angle with respect to the $H_u$ and $H_c$ axes. Away from this line $B$ has a downward trend.

In summary, the FORC function is concentrated around three lines that meet at 135° angles. One line ($H_c = 0$) is potentially significant beyond the Stoner-Wohlfarth model (Section IV B), one ($H_u = 0$) reflects a symmetry of Stoner-Wohlfarth hysteresis, and one ($H_a = -H_K/2$) comes from the angular dependence of the switching field in the Stoner-Wohlfarth model. The greatest concentration is around the two meeting points at $(H_c, H_u) = (0, H_K/2)$ and $(H_c, H_u) = (H_K/2, 0)$. The spread about these peaks along the ridges gives rise to the banana shape noted by[17].

As Fig. 4a shows, $f_h$ is antisymmetric about $h_b = 0$ for all particle orientations. Therefore, $B$ is also antisymmetric about $H_b = 0$ or $H_u = -H_c$, as can be seen in Fig. 7b. By contrast, $A$ is entirely on one side of this axis.

### C. Average over random orientations (anisotropic)

Suppose that some easy axis directions are more probable than others. If this anisotropy is modeled by a probability distribution, the distribution should be bimodal because each axis can be represented by two opposing directions. A simple example of such a distribution is the Dimroth-Watson distribution[12]:

$$\nu(\theta, \kappa) = b(\kappa) \exp(\kappa \cos^2 \theta), \tag{21}$$

where

$$b(\kappa) = \left( 2 \int_0^1 \exp(\kappa t^2) dt \right)^{-1}. \tag{22}$$

When $\kappa = 0$ this reduces to the isotropic distribution. If $\kappa > 0$ the axes are concentrated around the field direction ($\theta = 0$) and if $\kappa < 0$ they are more towards the perpendicular.

For a sample with this distribution (14) is replaced by

$$\tilde{\mu}(h_a, h_b) = \int_0^{\pi/2} \tilde{\mu}(\theta, h_a, h_b) \nu(\theta, \kappa) \sin\theta d\theta. \tag{14c'}$$

The calculation of $\tilde{\mu}$ is similar to that in Section III B, and the result is the same except that (19c) is replaced by

$$g(\theta, h) = f(\theta, h) \nu(\theta, \kappa) \sin\theta. \tag{19'}$$

The anisotropic FORC function is plotted in Fig. 8 for a sample with a prolate ($\kappa > 0$) distribution. Because a prolate distribution weights small angles more heavily than large angles, the negative region in $A$ (Section III B) disappears.

The anisotropy acts through the critical angle $\theta_a \equiv \theta_s(h_a)$, so its main effect is to redistribute the FORC

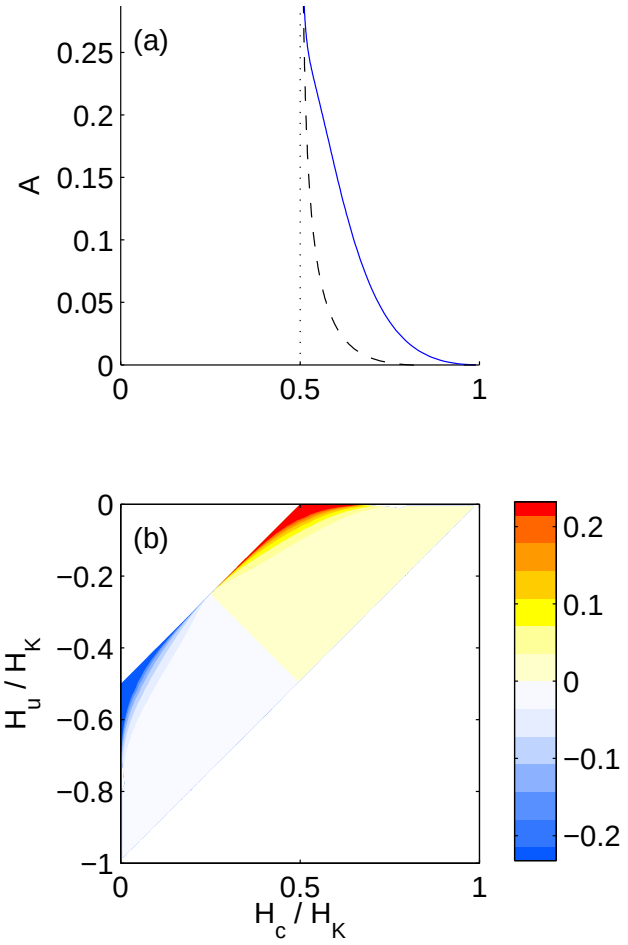


FIG. 8: The components of the FORC function for identical particles with an anisotropic distribution of orientations given by the Dimroth-Watson distribution $\nu(\theta,\kappa)$ with $\kappa = 5$. Same conventions as in Fig. 7. (a) $A$, with the isotropic case (dashed line) for comparison. (b) $B$.

function in the $h_a$ direction. However, the redistribution also depends on $h_b$ because of (19b) and it changes the balance between $A$ and $B$. The integral of $A$ over the plane is

$$\begin{aligned} m_j &= \int_{-\infty}^{\infty} dh_a \int_{-\infty}^{\infty} \alpha(h_a)\delta(h_a + h_b)dh_b \\ &= \int_0^{\pi/2} f(\theta, h_s(\theta))\nu(\theta,\kappa)\sin\theta d\theta. \end{aligned} \tag{23}$$

Since $B$ is symmetric about $h_b = 0$ its integral over the entire plane is zero. However, its integral over positive $h_b$ is

$$m_{sl} = \int_0^{\pi/2} \left[f(\theta,0) - f(\theta,h_s(\theta))\right]\nu(\theta,\kappa)\sin\theta d\theta, \tag{24}$$

while the integral over negative $h_b$ is $-m_{sl}$. Now $f(\theta,0) = 2\cos\theta$ is just the difference between the positive and negative remanences for a single particle. Its

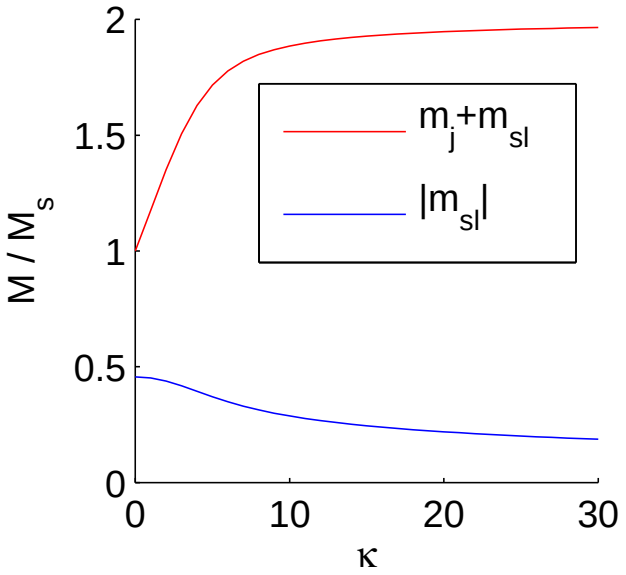


FIG. 9: The integrals of the FORC function over $H_b > 0$ ($m_j + m_{sl} = 2M_{rs}/M_s$) and $H_b < 0$ ($m_{sl}$) as a function of the Dimroth-Watson parameter $\kappa$.

integral over $\theta$ is $m_j + m_{sl} = 2M_{rs}/M_s$. Thus, $m_j$ is the contribution of jumps to the total change in remanence while $m_{sl}$ is the net effect of traveling up one curve and down another in each particle. Alternatively, $m_j + m_{sl}$ and $m_{sl}$ are the relative weights of the positive and negative regions.

The magnetizations $m_j + m_{sl}$ and $m_{sl}$ are shown in Fig. 9. The value of $M_{rs}/M_s$ at $\kappa = 0$ is 0.5, agreeing with the classic Stoner-Wohlfarth result for an isotropic sample. As $\kappa$ increases the easy axes become more concentrated about the field direction and $M_{rs}/M_s$ approaches unity. Meanwhile $m_{sl}$ starts at 0.47 and decreases to zero. (If all the axes are parallel to the field none of the change in magnetization is reversible.) Clearly the positive part of the FORC function always dominates the negative part. The ratio $(m_j + m_{sl})/m_{sl}$ is at least 2.2 and decreases as $\kappa$ increases.

### D. Average over anisotropy field $H_K$

In a real material the magnetic particles are not identical. Suppose that the anisotropy field $H_K$ varies. Let $H_K = NM_s$, where $N$ is dimensionless. $N$ may be the shape-dependent demagnetizing factor (Appendix A) or an effective demagnetizing factor representing magnetoelastic anisotropy. Suppose that $N$ is always positive and has a probability density function $\rho_N(N)$. This pdf must satisfy $\rho_N(N) \geq 0$ and $\int_0^\infty \rho_N(N)dN = 1$.

The FORC function is obtained by integrating the

function for identical particles (8) over $N$:

$$\mu(\rho_N|H_a,H_b)=\frac{1}{M_s}\int_0^\infty \tilde{\mu}(\frac{H_a}{NM_s},\frac{H_b}{NM_s})\rho_N(N)\frac{dN}{N^2}. \tag{25}$$

The integrand is only nonzero for $N_1 \le N \le N_2$, where $N_1 = |H_a|/M_s$ and $N_2 = \min(1/2, 2|H_a|/M_s)$ (see Appendix A). The new coefficients are

$$A(\rho_N|H_a)=\int_{N_1}^{N_2}\alpha(\frac{H_a}{NM_s})\rho_N(N)\frac{dN}{N} \tag{26a}$$

$$B(\rho_N|H_a,H_b)=\int_{N_1}^{N_2}\beta(\frac{H_a}{NM_s},\frac{H_b}{NM_s})\rho_N(N)\frac{dN}{N^2}. \tag{26b}$$

The theory in this article applies only to particles with uniaxial anisotropy, but many geologically interesting materials such as magnetite have a cubic magnetocrystalline anisotropy. Fortunately, the cubic anisotropy can be neglected if the particles are elongated. For such particles it is best to start with a pdf for the particle aspect ratio $q$ and use it to derive the pdf for the demagnetizing factor (Appendix A). The integral is evaluated using adaptive Gauss/Lobatto quadrature[8] with a relative accuracy of $10^{-6}$ or better.

Many of the properties of a system of identical particles are still true of a system with a shape distribution. For example, in a set of identical particles, $B(H_a,-H_b) = -B(H_a,H_b)$. In (26) this implies that $B(\rho_N|H_a,-H_b) = -B(\rho_N|H_a,H_b)$. Thus, the antisymmetry of $B$ about $H_u = -H_c$ is preserved. Also, the positive and negative peaks have the same relative weights as in Section III C.

The arguments are plotted in Fig. 10 for a lognormal distribution of aspect ratios with mean $\bar{q} = 2$, corresponding to a demagnetizing factor $N_0(\bar{q}) = 0.24$. Equation 26b predicts that the shape distribution will spread the FORC function equally in all directions, and this is consistent with Fig. 10. One result of this spreading is that the slanted ridges are replaced by humps that are roughly symmetric about the peaks.

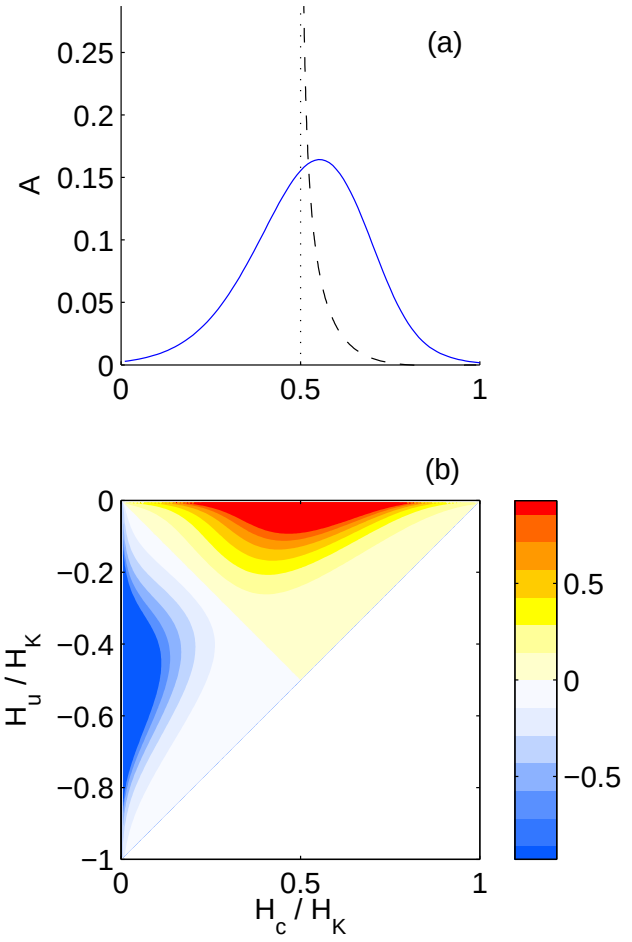


FIG. 10: The components of the FORC function an isotropic sample with a lognormal distribution of aspect ratios ($\overline{q} = 2$ and $\sigma = 0.25$). (a) $A$. The function for identical particles with aspect ratio $\overline{q}$ is shown as a dashed line. (b) $B$. The same color scale is used as in Fig. 3.

### E. Comparison With Experiment

The theory developed in this article has some specific predictions for the FORC function of a sample with uniaxial SD particles. The function is nonzero only for $H_c > 0$ and $H_u < 0$. It has a sharp positive maximum on the $H_c$ axis and a sharp negative minimum at an equal distance down the $H_u$ axis from the origin. The positive peak is larger than the negative peak, the difference in size depending on the anisotropy. If the shape distribution is narrow a ridge extends from each peak at a 45° angle, but as the shape distribution gets wider the ridge smears out into a hump.

Before comparing these predictions with the experimental FORC function in Fig. 3, I will estimate the distribution parameters for the magnetic tape. It has a saturation remanence ratio $M_{rs}/M_s = 0.62$, which corresponds to a Dimroth-Watson distribution with $\kappa = 1.4$ (Fig. 9). The shape distribution parameters can be estimated by fitting a direct field (DF) demagnetization curve, which can be derived from the FORCs as follows. For each FORC that crosses $H_b = 0$, interpolate to get the magnetization $M_{df}(H_a) = M(H_a, 0)$. Since $H_a$ is the minimum field on this FORC, $M_{df}(H)$ is the DF demagnetization curve. The method for fitting this curve to the theoretical $M_{df}$ is described in Appendix B. The best fit ( Fig. 11) is for a mean aspect ratio $\bar{q} = 2.6$ and a standard deviation $\sigma = 0.4$. The fit is quite good. However, it is unlikely that the aspect ratios are really as low as 2.6. When elongated particles are used in magnetic tapes the aspect ratios are closer to $10^{15}$.

The theoretical FORC function plotted in 10 uses parameters for the shape distribution that are close to the values fitted to the remanence curve. Some features agree well with the FORC function for the magnetic tape. Both have a negative peak near the $H_u$ axis at the same dis-

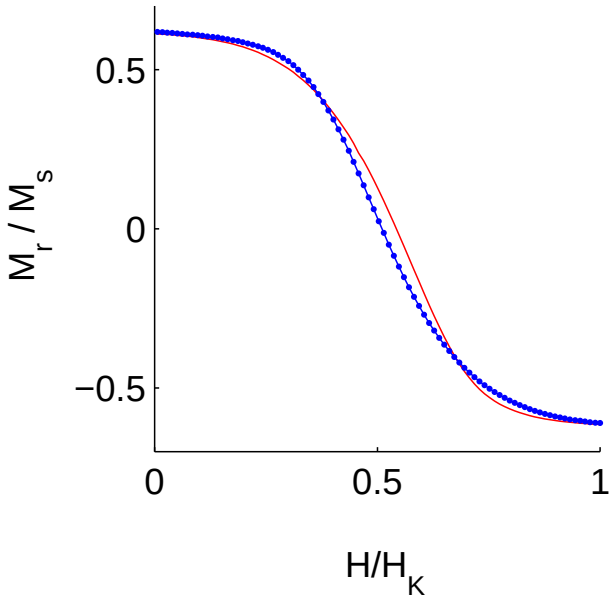


FIG. 11: The DF demagnetization curve derived from the FORCs (points) and the best-fitting theoretical curve (red line).

tance from the origin as the positive peak. This distance is $0.5H_K$, where $H_K$ is the field at which the hysteresis loop closes.

As the theory predicts, the positive peak is larger than the negative peak. The integral over the positive region $(m_j + m_{sl})$ can be estimated by interpolating the data onto a regular grid and using Simpson integration. The result is 0.60, which agrees well with $2M_{rs}/M_s$. However, the theory predicts that $\mu$ is nonzero only for $H_b \leq -H_a$, and the integral over $0 \leq H_b \leq -H_a$ is only 0.37. The integral over the negative region is $-0.08$, which has a much smaller magnitude than the theoretical value of $-0.45$.

Some qualitative features of Fig. 3 do not agree with the theory. The boundary between the positive and negative regions does not lie along $H_u = -H_c$, but this may be because the small values of $\mu$ are not statistically significant. A ridge extends from the negative peak towards the positive peak, more like a narrow size distribution than one with $\sigma = 0.4$; and the positive peak does not have a clear ridge. (The positive peak in[1] looks more like the theoretical prediction.) However, these are all small differences compared to the most obvious difference: Instead of being zero for $H_u > 0$, the positive peak is nearly symmetric about the $H_c$ axis. I will discuss possible reasons for this disagreement in Section IV C.

## IV. DISCUSSION

In this section I first discuss some of the properties of the theoretical FORC function and then discuss the most important disagreement between theory and experiment. One property of the theoretical function is that it violates the symmetry $\mu(-H_c, H_u) = \mu(H_c, H_u)$ required by classical Preisach theory[14]. In section IV A I discuss this symmetry violation and its relationship to the dual definition of $\mu$ for increasing and decreasing FORCs. The negative region is one of the surprises to come out of plotting experimental FORC functions. I clarify its physical significance in section IV B. Finally, in section IV C I discuss the possible reasons for the symmetric spreading of the positive peak about the $H_c$ axis.

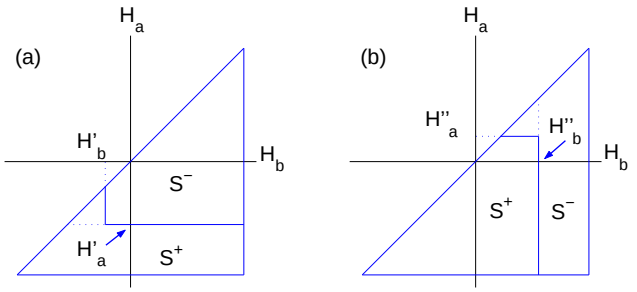


FIG. 12: The positive ($S^+$) and negative ($S^-$) regions on the Preisach diagram for the FORCs in Fig. 2. (a) Increasing FORCs. (b) Decreasing FORCs.

### A. Asymmetry of $\mu$

Classical Preisach theory requires that the function have the symmetry

$$\mu(-H_b, -H_a) = \mu(H_a, H_b), \tag{27}$$

which is a reflection symmetry about the $H_c$ axis on a FORC diagram. FORC functions of real samples often do not have this symmetry. What is the significance of this symmetry requirement? And why is the definition of $\mu$ different for increasing and decreasing FORCs (equations 1-2)?

Preisach theory represents hysteresis as the weighted sum of units of hysteresis, or hysterons. Each hysteron has outputs of either $+1$ or $-1$. A hysteron associated with the point $(H_a, H_b)$ has a downward jump at $H_a$ and an upward jump at $H_b$. The region where the weights are nonzero is called the support. The support is divided into subregion $S^+$ containing all the hysterons in the $+1$ state, and $S^-$ containing all the negative hysterons[14]. The magnetization is an integral over these regions:

$$M = \iint_{S^+} \mu(x,y)dxdy - \iint_{S^-} \mu(x,y)dxdy. \tag{28}$$

The subregions change as the magnetic field changes (Fig. 12). At positive saturation $S^+$ fills the entire support. As $H$ decreases to $H'_a$, hysterons in the region $H_a > H'_a$ switch to the negative state. This is represented by a horizontal line that sweeps down, changing

$S^+$ to $S^-$. When the field increases from $H'_a$ to $H'_b$, hysterons with $H_b < H'_b$ switch back. This is represented by a vertical line sweeping to the right. The result, the Preisach state for the point $M(H'_a, H'_b)$ on an increasing FORC, is shown in Fig. 12a. The Preisach state for a point$M(H''_a, H''_b)$ on a decreasing FORC is shown in Fig. 12b.

For Preisach theory to work, a FORC function derived from increasing FORCs must correctly predict decreasing FORCs. Preisach theory assumes that increasing and decreasing FORCs are congruent (that is, $M(-H_b, -H_a) = -M(H_a, H_b)$). If $H''_a = -H'_b$ and $H''_b = -H'_a$ the integral over $S^-$ in Fig. 12a must be the same as the integral over $S^+$ in Fig. 12b. This can only be true in general if $\mu$ is symmetric across the line $H_b = -H_a$, that is, (27) holds for all $H_a$ and $H_b$. If $\mu$ is defined by (1) for increasing FORCs, the above symmetries require that $\mu$ be defined by (2) for decreasing FORCs.

Why should $M(-H'_b, -H'_a)$ be equal to $-M(H'_a, H'_b)$? On this point, Preisach theories are vague, perhaps because the reason depends on the physical origin of the hysteresis. In magnetic systems, it follows from the invariance of Maxwell's equations under time reversal[10]. Any solution of Maxwell's equations for time moving forward should still be a solution if time moves backwards. Time reversal changes the signs of $\mathbf{M}$ and $\mathbf{H}$, so for every solution $(\mathbf{M}, \mathbf{H})$ there should be another solution $(-\mathbf{M}, -\mathbf{H})$. This is inversion symmetry.

In general there is an increasing FORC function $\mu^i$ and a different decreasing FORC function $\mu^d$. Because of inversion symmetry these functions are images of each other by reflection across the $H_c$ axis. If they both have the symmetry (27) then they are identical and the classical Preisach function is well defined ($\mu \equiv \mu^i \equiv \mu^d$). If not, Maxwell's equations still apply but classical Preisach theory cannot predict the magnetization correctly.

Classical Preisach theory correctly predicts hysteresis if and only if the hysteresis has certain properties[13]. One property is that all hysteresis loops between a given pair of field extrema are geometrically congruent. The hysteresis of Stoner-Wohlfarth particles does not have this property. For example, in Fig. 4, if the extrema are $h_1$ and $h_2$, with $-h_s < h_1 < h_2 < h_s$, there are two possible loops depending on the initial state. If the magnetization starts on the upper curve, the magnetization goes back and forth reversibly on the upper curve. The alternative is a loop that follows the lower curve. Fig. 4a shows that there can be an arbitrarily large difference in slope between the two curves, so they are not congruent. This difference in slope is represented by component $B$ in the FORC function, and it is $B$ that violates the symmetry condition.

At least $B$ contains some information on the magnetic hysteresis. Other information is lost. $B$ only records the difference in slopes between two magnetization curves, but the FORC function cannot tell us the slope of either curve by itself. In addition, the saturation magnetization is lost. These losses occur because the FORC function is obtained by taking two derivatives of the magnetization $M(H_a, H_b)$. To recover $M$ one must integrate twice, which introduces two unknown integration constants. However, the information loss has an advantage. Paramagnetic and superparamagnetic components are removed, isolating the hysteresis. The FORC function also highlights regions where the hysteresis has a large effect on the magnetization.

### B. Negative functions

As mentioned in Section I, Preisach modelers often assume that the Preisach function is a probability density. However, this assumption is contradicted by the negative region in Fig. 3 and in other single-domain samples[1,26]. The negative region does not violate any necessary condition for Preisach theory. Indeed, negative Preisach functions can be related to observable features of first-order reversal curves[14].

In Preisach theory, a negatively weighted hysteron is simply an upside-down hysteris loop, having an upward jump for decreasing field and a downward jump for increasing field. Those familiar with Preisach theory may find this disturbing, and they have a good physical reason for their disquiet. A negative hysteresis loop cannot exist by itself because it performs net work on the field. However, the hysteresis loop for a Stoner-Wohlfarth particle is represented by a distribution of hysterons, and in a circuit around the loop the field does net work on the particle. Negatively weighted hysterons are a reminder that the hysterons do not have a simple physical meaning.

The negative part of $A$ comes from jumps in the direction of the field, as in Fig. 5. This only occurs in particles with easy axes nearly perpendicular to the field. The negative part of $B$ comes from the difference in slopes near a jump. Almost all particles contribute to $B$ (the exception being those with easy axes parallel to the field). As the field approaches a jump the slope of the magnetization curve increases to infinity. After the jump the slope is finite again. If the jump is from a lower curve to an upper curve ($H_b = -H_a$ in the Stoner-Wohlfarth model), the FORC function approaches positive infinity at the jump. If the jump is the other way ($H_b = H_a$), the FORC function approaches negative infinity. (A similar interpretation was offered by[25], but it was based on a hypothetical form for a hysteron and there was no approach to infinity.)

The approach to infinity of the slope is a "generic" feature of instabilities that occur in many physical systems[9,21,22]. It is associated with the convergence and mutual annihilation of a stable state and an energy barrier. Thus, in any magnetic system the difference between slopes should always make a negative contribution to the FORC function.

If there is always a negative contribution to the FORC function near $H_a = H_b$, why is it not seen in all exper-

imental FORC diagrams? In larger particles it may be canceled out by small positive jumps. In larger particles large jumps are replaced by small Barkhausen jumps due to movement of domain walls over defects. In a system with many particles there is always an upward jump near any downward jump. Downward jumps contribute to the FORC function only through the difference in slopes, but upward jumps also contribute the height of the jump. Thus, the upward jumps hide the lower jumps and only a positive contribution is seen.

### C. The symmetric peak

I showed in Section III E that Stoner-Wohlfarth theory can fit a remanence curve for the magnetic tape quite well, but the aspect ratios deduced from this fit are implausible. Disagreement between theory and experiment is more obvious in the FORC function. In this section I discuss the most obvious disagreement, the spread of the positive peak to positive $H_u$.

One possible explanation for the spread of the peak is a numerical artifact. Experimental functions are based on polynomial fits to discrete measurements of $M(H_a, H_b)$. The field increments must be very small to represent some of the features of Stoner-Wohlfarth systems. Half the change in magnetic remanence occurs between $H = 0.5H_K$ and $H = 0.524H_K$, the latter being the coercivity of remanence[34]. Experimental FORC functions are derived from polynomial fits to $(2 * \mathrm{SF} + 1)^2$ points, where SF is called the smoothing factor. The same procedure is used by[17] to fit a FORC function to numerical simulations of FORC curves for Stoner-Wohlfarth particles. They get a positive peak that is nearly symmetric about the $H_c$ axis, aside from the boomerang shape of the lowest contours. This is superficially similar to the experimental FORC function. However, in this article I have shown analytically that the FORC function for Stoner-Wohlfarth particles is zero for $H_u > 0$. Thus, in their model the spreading of the peak must be a numerical artifact.

Numerical artifacts are probably not the reason for the spread of the peak in Fig. 3. The FORC function looks essentially the same for SF = 1 and SF = 5, aside from small-scale noise. Thus, the spread of the positive peak to $H_u > 0$ is probably due to a physical effect.

Three physical effects could give rise to some spreading. First, thermal fluctuations make jumps occur early[24]. This effect narrows hysteresis loops, which would move the FORC function to lower $H_c$. It also replaces a jump at a discrete switching field by a probability of a jump that increases continuously as the field approaches the switching field. Since the positive peak relates the upward jump to the downward jump, and both jumps spread independently, thermal fluctuations should spread the positive peak equally in the $H_c$ and $H_u$ directions. By contrast, the negative peak should spread mainly in the $H_a$ direction. Thermal fluctuations could account for some of the observed spreading, but the effect is probably too small. A large thermal effect would imply a strong temperature dependence of the FORC function, and the temperature dependence of the FORC functions in[1] is very weak. It is weak because probability distribution is generally tightly concentrated around an effective switching field. Compared to zero fluctuations, the switching field is reduced by a factor $1 - (V_{SP}/V)^x$, where $V_{SP}$ is the upper volume limit for superparamagnetism and $x$ is between 1.43 and $2^{24}$. The reduction is already less than 5% for a particle that is only twice the superparamagnetic limit in each dimension. The extent of spreading will be even less.

Second, particle interactions can spread the FORC function in the $H_u$ direction without having much effect on the $H_c$ direction[17]. Although this could account for some of the spreading in Fig. 3, particle interactions are undesirable in magnetic tapes. Thus, manufacturers try to keep the magnetic particles apart to reduce interactions.

Whether or not particle interactions are present, a third effect is unavoidable: non-SD magnetization change. The ratio $M_{rs}/M_s = 0.62$ is strong evidence for an SD saturation remanence, but that does not mean that the particle reverses by the SD mechanism of uniform rotation. Indeed, uniform rotation is unlikely.[20] calculated the upper size limit for uniform rotation and showed that it is never far from the upper limit for superparamagnetism, even the size range for SD saturation remanence is broad.

A particle with an SD saturation remanent state can also have a non-SD, or multidomain (MD), remanence after partial demagnetization.[21] showed that when a MD state has the lowest energy, new jumps and new loops appear in the hysteresis (indeed, these were the first micromagnetic simulations of FORCs). An example is shown in Fig. 13. In this example the saturation remanent state is not SD, but that is because the particle is not very elongated. There are three increasing FORCs, one for any field $H_a$ before the first jump (green), one for any $H_a$ between jumps (blue) and one after the second jump (red). Considering just the contribution of the jumps to the FORC function, the difference between the green and blue curves will contribute a delta function with $H_u > 0$. The difference between blue and red curves will contribute one delta function with $H_u < 0$ (first red jump) and one with $H_u = 0$ (second jump). The overall spreading is nearly symmetric, as one would expect of a system that has inversion symmetry in the $(\mathbf{H}, \mathbf{M})$ plane (section IV A).

## V. CONCLUSIONS

In general, a system with hysteresis has two FORC functions, one for increasing FORCs and one for decreasing FORCs. These functions are mirror images across the $H_c$ axis. If they both have reflection symmetry across

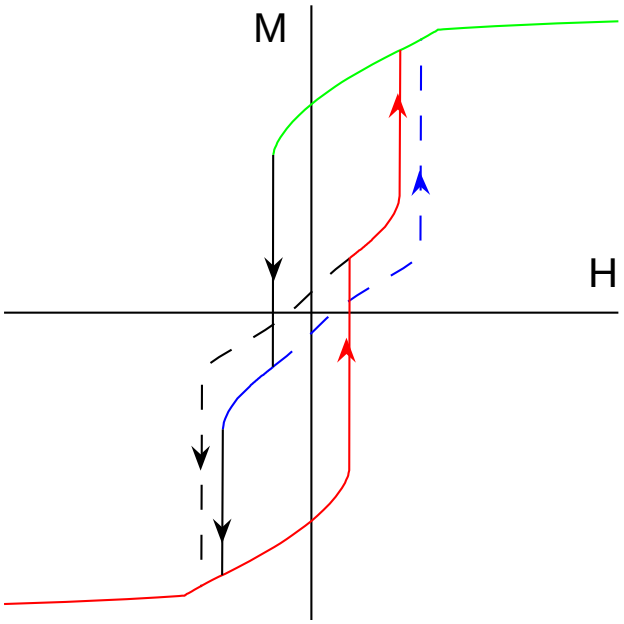


FIG. 13: The magnetic hysteresis for a magnetite particle with volume $(0.09\,\mu\text{m})^3$, a triaxial shape $X = 1.5Y = 1.4Z$ and a field in the $(8, 4, 1)$ direction. Arrows show the direction of jumps. The solid curve is the main hysteresis loop while the dashed lines are FORCs for fields after the first jump. The increasing FORCs are highlighted in green, blue and red. Adapted from Fig. 11 in[21].

this axis, they are the same and classical Preisach theory applies. However, they are not the same for systems of single-domain particles because each particle has upper and lower magnetization curves that are not congruent. Below, statements about the FORC function apply to increasing FORC functions.

The FORC function for a system of noninteracting, elongated single-domain particles has two parts. A delta function on the $H_c$ axis represents jumps in magnetization. A continuous function over $H_c > 0$ and $H_u < 0$ represents differences in slopes between the upper and lower magnetization curves for each particle. The latter has a positive peak on the $H_c$ axis and a negative peak on the negative $H_u$ axis. These peaks are at equal distances from the origin. From each peak a ridge extends along the axis away from the origin. Each peak also has a ridge slanting towards the other peak. This ridge is due to the strong dependence of the switching field on the angle between the easy axis and the field when that angle is near 45°.

The negative region is consistent with classical Preisach theory but inconsistent with assumptions that the FORC function is a probability distribution. It seems to violate conservation of energy, but on closer examination it does not. In all particles, not just SD, the difference between slopes before and after each downward jump should make a negative contribution to the FORC function. This region is probably not seen in larger particles because it is canceled by nearby upward jumps.

If the particles are identical but have an anisotropic distribution of easy axis orientations, the above qualitative features are not changed but the balance between jumps and slope differences is altered. This also changes the balance between the positive and negative regions. In the extreme case of all particles being aligned with the field, all the magnetization change comes from jumps and there is no negative peak.

If the particles have a distribution of shapes the appearance of the FORC function changes. The function becomes more symmetric about each peak and the slanted ridges disappear.

It is much harder to fit distribution parameters using FORC functions than using remanence curves, but the latter turn out to underestimate the aspect ratios of the particles in the magnetic tape. Discrepancies between theory and experiment are more obvious in the FORC function. Most importantly, the theory predicts that the FORC function should be zero for $H_u > 0$, but experimental FORC functions for SD particles are nearly symmetric about this axis. The most likely reason for this disagreement is that the nominally SD particles can have multidomain remanent states. This is not apparent in the ratio $M_{rs}/M_s$ because the saturation magnetization state is SD.

## APPENDIX A: A PROBABILITY DENSITY FUNCTION FOR THE DEMAGNETIZING FACTOR

In this Appendix I derive an expression for the probability density function (pdf) of the demagnetizing factor $N$ given a probability function for the aspect ratio of a spheroid. The aspect ratio is defined as $q = a/b$, where $a$ is the major axis and $b$ is the minor axis of the ellipsoid. For a prolate ellipsoid the demagnetizing factor is given by[2]

$$N = \frac{1}{2} - \frac{3}{2} q (q^2 - 1)^{-3/2} \cosh^{-1} q - \frac{3}{2} (q^2 - 1)^{-1}. \quad \text{(A1)}$$

As $q$ goes from one to infinity, $N$ starts at zero and approaches an asymptote of $1/2$.

Suppose that the aspect ratio $q$ has a pdf $\rho_q(q)$. The corresponding pdf for the demagnetizing factor is given by[28]

$$\rho_N(N) = \frac{1}{|N'(q(N))|} \rho_q(q(N)), \quad \text{(A2)}$$

where $q(N)$ is the inverse of the function $N(q)$ and $N'(q)$ is the first derivative of $N(q)$.

In evaluating the integrals in (26), one must take care to restrict $H_a$ and $H_b$ to the region where the density is nonzero. Otherwise, $N$ can be out of bounds and $q(N)$ will be undefined. Combining the integral limits $-1 \le h \le -1/2$ with $0 \le N \le 1/2$ and $h = H_a/NM_s$, we get $-M_s/2 \le H_a \le 0$. In addition the upper integral limit

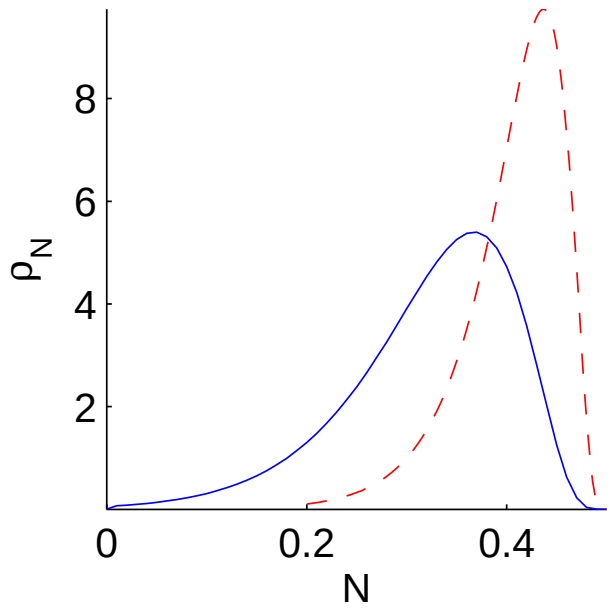


FIG. 14: Probability density functions for the demagnetizing factor $N$ derived from lognormal densities of the grain aspect ratio $q$. The solid and dashed lines both have the same standard deviation $\sigma = 0.4$, but the pdf for $\overline{q} = 5$ (solid line) is narrower than the pdf for $\overline{q} = 3$ (dashed line) because $N$ approaches a limit of 0.5 for large $q$.

must be changed to $N_2 = \min(1/2, 2|H_a|/M_s)$. Finally, $|H_b| \leq |H_a|$. Outside of this region the FORC function is zero.

An example of functions $\rho_N$ generated using a lognormal function $\rho_q(N, \overline{q}, \sigma)$ is plotted in Fig. 14. Because $N$ approaches a limit of 0.5 as $q$ approaches infinity, $\rho_N$ gets narrower as the mean $q$ increases even if the standard deviation remains the same. The distribution is also skewed upwards.

## APPENDIX B: FITTING THE DF DEMAGNETIZATION CURVE

The saturation remanence for an anisotropic sample of identical particles is given by $(m_j + m_{sl})/2$ (Section III C), or

$$M_{rs} = \int_0^{\pi/2} \nu(\theta, \kappa) \cos\theta \sin\theta d\theta, \tag{B1}$$

and this remanence is independent of the shape distribution.

For identical particles with easy axis orientations given by the Dimroth-Watson distribution, the normalized remanence after AF demagnetization in a peak alternating field $H = hH_K$ given by[19]

$$\frac{M_{af}(h,\kappa)}{M_{rs}} = 1 - \cos^2\theta_s(h) + \sin^2\theta_s(h) \tag{B2}$$

for $\kappa = 0$, and

$$\frac{M_{af}(h,\kappa)}{M_{rs}} = 1 - \frac{\exp(\kappa\cos^2\theta_s(h)) - \exp(\kappa\sin^2\theta_s(h))}{\exp(\kappa) - 1} \tag{B3}$$

for $\kappa \neq 0$.

If the particles have a shape distribution, the AF demagnetization curve is given by the integral

$$M_{af}(\rho_N|H,\kappa) = \int_{H/M_s}^{0.5} M_{af}\left(\frac{H}{N},\kappa\right)\rho_N(N)dN. \tag{B4}$$

The above expressions can also be combined with the Wohlfarth relations for uniaxial SD particles[37]

$$M_{ir}(H) = M_{rs} - M_{af}(H) \tag{B5a}$$
$$M_{df}(H) = 2M_{af}(H) - M_{rs}, \tag{B5b}$$

to calculate the IRM acquisition curves $M_{ir}(H)$ and direct field (DF) demagnetization curves $M_{df}(H)$.

The value for $\kappa$ is obtained by finding the value that makes $m_j + m_{sl}$ equal to the measured value of $2M_{rs}/M_s$. This can be done adequately by interpolation. Given $\kappa$ and an estimate for $M_{df}(H)$ from the FORCs, the parameters of the shape distribution are estimated using a nonlinear Gauss-Newton least squares algorithm (implemented in Matlab® ).

## ACKNOWLEDGMENTS

I would like to thank Chris Pike for many valuable comments on this manuscript and for the magnetic tape data. Reviews by Adrian Muxworthy and Stephen Park also led to significant improvements in the manuscript.

* Andrew_Newell@ncsu.edu; http://www4.ncsu.edu/~ajnewell/index.html

[1] Carvallo, C., O. Özdemir, and D. J. Dunlop (2004), First-order reversal curve (FORC) diagrams of elongated single-domain grains at high and low temperatures, *J. Geophys. Res.*, *109*, B04,105, doi:10.1029/2003JB002539.
[2] Chikazumi, S. (1997), *Physics of Ferromagnetism*, Oxford, New York, 655 pp.
[3] Day, R., M. Fuller, and V. A. Schmidt (1977), Hysteresis properties of titanomagnetites: grain-size and compositional dependence, *Phys. Earth Planet. Inter.*, *13*, 260–267.
[4] Della Torre, E. (c1999), *Magnetic hysteresis*, IEEE Press, New York, 215 p.
[5] Dunlop, D. J., and O. Özdemir (1997), *Rock Magnetism:*

*Fundamentals and Frontiers*, Cambridge Univ. Press, New York, 573 pp.

[6] Egli, R. (2003), Analysis of the field dependence of remanent magnetization curves, *J. Geophys. Res.*, *108*, 2081, doi:10.1029/2002JB002023.

[7] Feinberg, J. M., H. R. Wenk, P. R. Renne, and G. R. Scott (2004), Epitaxial relationships of clinopyroxene-hosted magnetite determined using electron backscatter diffraction (EBSD) technique, *Am. Mineral.*, *89*, 462–466.

[8] Gander, W., and W. Gautschi (2000), Adaptive quadrature - revisited, *BIT*, *40*(1), 84–101.

[9] Iooss, G., and D. D. Joseph (1990), *Elementary Stability and Bifurcation Theory*, 2nd ed., Springer-Verlag, New York, 324 pp.

[10] Jackson, J. D. (1975), *Classical Electrodynamics*, John Wiley and Sons, 848 pp.

[11] Jackson, M. (1990), Diagenetic sources of stable remanence in remagnetized Paleozoic cratonic carbonates: A rock magnetic study, *J. Geophys. Res.*, *95*, 2753–2761.

[12] Mardia, K. V. (1972), *Statistics of Directional Data*, Academic Press, New York, NY, 357 pp.

[13] Mayergoyz, I. D. (1986), Mathematical models of hysteresis, *Phys. Rev. Lett.*, *56*(15), 1518–1521.

[14] Mayergoyz, I. D. (1991), *Mathematical Models of Hysteresis*, Springer-Verlag.

[15] Mee, C. D., and E. D. Daniel (Eds.) (1996), *Magnetic Storage Handbook*, 2nd ed., McGraw-Hill.

[16] Messiah, A. (c1962), *Quantum Mechanics*, vol. 1-2, John Wiley & Sons, translated from the French by G. M. Temmer. 1136 pp.

[17] Muxworthy, A., D. Heslop, and W. Williams (2004), Influence of magnetostatic interactions on first-order-reversal-curve (FORC) diagrams: a micromagnetic approach, *Geophys. J. Int.*, *158*, 888–897, doi:10.1111/j.1365-246X.2004.02358.x.

[18] Muxworthy, A. R., and D. J. Dunlop (2002), First-order reversal curve (FORC) diagrams for pseudo-single-domain magnetites at high temperature, *Earth Planet. Sci. Lett.*, *203*, 369–382.

[19] Newell, A. J. (2000), The Lowrie-Fuller test: Single-domain and micromagnetic theory, *Earth Planet. Sci. Lett.*, (In press).

[20] Newell, A. J., and R. T. Merrill (1999), Single-domain critical sizes for coercivity and remanence, *J. Geophys. Res.*, *104*, 617–628.

[21] Newell, A. J., and R. T. Merrill (2000), Nucleation and stability of remanent states, *J. Geophys. Res.*, *105*, 19,377–19,391.

[22] Newell, A. J., and R. T. Merrill (2000), Size dependence of hysteresis properties of small pseudo-single-domain grains, *J. Geophys. Res.*, *105*, 19,393–19,403.

[23] Parry, L. G. (1982), Magnetization of immobilized particle dispersions with two distinct particle sizes, *Phys. Earth Planet. Inter.*, *28*, 230–241.

[24] Pfeiffer, H. (1990), Determination of anisotropy field distribution in particle assemblies taking into account thermal fluctuations, *phys. status. solidi. A*, *118*, 295–306.

[25] Pike, C. R. (2003), First-order reversal-curve diagrams and reversible magnetization, *Phys. Rev. B*, *68*, 104,424.

[26] Pike, C. R., A. P. Roberts, and K. L. Verosub (1999), Characterizing interactions in fine magnetic particle systems using first order reversal curves, *J. Appl. Phys.*, *85*, 6660–6667.

[27] Pike, C. R., A. P. Roberts, M. J. Dekkers, and K. L. Verosub (2001), An investigation of multi-domain hysteresis mechanisms using FORC diagrams, *Phys. Earth Planet. Inter.*, *126*, 11–25.

[28] Rice, J. A. (1995), *Mathematical Statistics and Data Analysis*, 2nd ed., Duxbury Press, Belmont, CA.

[29] Roberts, A. P., C. R. Pike, and K. L. Verosub (2000), First-order reversal curve diagrams: A new tool for characterizing the magnetic properties of natural samples, *J. Geophys. Res.*, *105*, 29,461–28,475.

[30] Robertson, D. J., and D. E. France (1994), Discrimination of remanence-carrying minerals in mixtures, using isothermal remanent magnetisation acquisition curves, *Phys. Earth Planet. Inter.*, *82*, 223–234.

[31] Selkin, P. A., J. S. Gee, L. Tauxe, W. P. Meurer, and A. J. Newell (2000), The effect of remanence anisotropy on paleointensity estimates: a case study from the Archean Stillwater Complex, *Earth Planet. Sci. Lett.*, *183*(3–4), 403–416.

[32] Song, T., and R. M. Roshko (2000), A Preisach model for systems with magnetic order, *Physica B*, pp. 24–27.

[33] Stancu, A., C. Pike, L. Stoleriu, P. Postolache, and D. Cimpoesu (2003), Micromagnetic and Preisach analysis of the First Order Reversal Curves (FORC) diagram, *J. Appl. Phys.*, *93*(10), 6620–6622.

[34] Stoner, E. C., and E. P. Wohlfarth (1948), A mechanism of magnetic hysteresis in heterogeneous alloys, *Philos. Trans. R. Soc. London Ser. A*, *240*, 599–642.

[35] Tauxe, L., T. A. T. Mullender, and T. Pick (1996), Potbellies, wasp-waists, and superparamagnetism in magnetic hysteresis, *J. Geophys. Res.*, *101*, 571–583.

[36] Vajda, F., and E. Della Torre (1991), Measurements of output-dependent Preisach functions, *IEEE Trans. Magn.*, *27*(6), 4757–4762.

[37] Wohlfarth, E. P. (1958), Relations between different modes of acquisition of the remanent magnetization of ferromagnetic particles, *J. Appl. Phys.*, *29*, 595–596.